Non-Orthogonal Multiple Access and Carrierless Amplitude Phase Modulation for Flexible Multi-User Provisioning in 5G Mobile Networks

Jose Antonio Altabas, Simon Rommel, *Student Member, IEEE*, Rafael Puerta, *Student Member, IEEE*,
David Izquierdo, Juan Ignacio Garces, *Member, IEEE*, Jose Antonio Lazaro, *Member, IEEE*,
Juan José Vegas Olmos, *Senior Member, IEEE*, and Idelfonso Tafur Monroy, *Senior Member, IEEE*

Abstract—In this paper, a combined non-orthogonal multiple access (NOMA) and multiband carrierless amplitude phase modulation (multiCAP) scheme is proposed for capacity enhancement of and flexible resource provisioning in 5G mobile networks. The proposed scheme is experimentally evaluated over a W-band millimeter wave radio-over fiber system. The evaluated NOMA-CAP system consists of six 1.25 GHz multiCAP bands and two NOMA levels with quadrature phase shift keying and can provide an aggregated transmission rate of 30 Gbit/s. The proposed system can dynamically adapt to different user densities and data rate requirements. Bit error rate performance is evaluated in two scenarios: a low user density scenario where the system capacity is evenly split between two users and a high user density scenario where NOMA and multiCAP are combined to serve up to twelve users with an assigned data rate of 2.5 Gbit/s each. The proposed system demonstrates how NOMA-CAP allows flexible resource provisioning and can adapt data rates depending on user density and requirements.

Index Terms—Non-orthogonal multiple access, multi-band carrierless amplitude phase modulation, radio-over-fiber, millimeter-wave communications, W-band wireless.

I. INTRODUCTION

TRAFFIC demand over wireless networks is growing exponentially due to new multimedia streaming services, the Internet of Things (IoT) and machine-to-machine communications [1]–[4]. These high bandwidth multi-gigabit wireless connections require 5G access networks that not only use the current and congested wireless bands but also the

J. A. Altabas, D. Izquierdo and J. I. Garces are with the Department of Electrical Engineering and Communications, Aragon Institute of Engineering Research, University of Zaragoza, 50018 Zaragoza, Spain, e-mail: jaltabas@unizar.es.

S. Rommel and R. Puerta are with the Department of Photonics Engineering, Technical University of Denmark, 2800 Kgs. Lyngby, Denmark, e-mail: sirem@fotonik.dtu.dk.

D. Izquierdo is also with the Centro Universitario de la Defensa, 50090 Zaragoza, Spain.

J. A. Lazaro is with the School of Telecommunications Engineering, Polytechnic University of Catalonia, 08034 Barcelona, Spain.

J. J. Vegas Olmos is with Mellanox Technologies, 4000 Roskilde, Denmark.

I. Tafur Monroy is with the Institute for Photonics Integration, Eindhoven University of Technology, 5600 MB Eindhoven, Netherlands.

millimeter wave (mm-wave) bands such as IEEE V- (40–75 GHz) and W-bands (75–110 GHz) [3]–[8]. The V-band has been proposed for indoor communications and next generation Wi-Fi due to the atmospheric oxygen absorption peak [7], [9] while the W-band presents a lower atmospheric absorption [7] and is thus favored for both indoor and outdoor wireless communications.

The introduction of mm-wave frequencies to 5th generation mobile communications requires a re-design of front- and backhaul radio access network (RAN) architectures, to enable them support high data rates, heterogeneous user density scenarios and flexible resource provisioning [2]. The use of centralized radio access networks (C-RANs) is suggested as a key enabler [3], [4], [8], which, combined with radio-over-fiber (RoF) on passive optical networks (PONs), is a promising candidate to flexibly support 5G mobile networks [8], [10].

In RANs, the design of the access to the medium is essential to improve the system capacity and to dynamically allocate the available resources. Non-orthogonal multiple access (NOMA) is a promising candidate for addressing these requirements and to enhance both capacity and flexibility of the network [11]–[16]. NOMA uses power multiplexing as a multiple access approach, allowing a direct sharing of time and frequency resources between users. NOMA can also improve the spectral efficiency of the RAN, allowing massive connectivity, low transmission latency and low cost [11], [14], [15].

In addition, high data rate demands require a migration from inefficient modulation formats, such as impulse radio or on-off keying, to advanced and flexible modulation schemes such as multi-band orthogonal frequency division multiplexing (MB-OFDM) [17] or multi-band carrierless amplitude phase (multiCAP) modulation [18]. Although MB-OFDM has shown flexible adaptation to a dynamically changing wireless medium, multiCAP allows less complex transceivers [19] and has shown promising results [20]–[23], achieving large capacities even under difficult channel conditions.

In this paper, both NOMA and multiCAP techniques are combined in order to allow flexible resource provisioning, able to address the dynamic nature of user density and capacity demands. This proposed NOMA-CAP combination can be a feasible technique for the standardization of the future 5G networks.

Fig. 1(a) shows a scenario of only two users at different distances to the base station (BS). A high capacity link will be

Fig. 1. NOMA-CAP multiplexing scenarios with different user densities.

Fig. 2. NOMA constellation multiplexing for two users with QPSK signals.

assigned to each by means of sharing all multiCAP bands using NOMA multiplexing. When new users try to access the RAN, the resources can be flexibly allocated, assigning different multiCAP bands to different users, as shown in Fig. 1(b). In this high density scenario, NOMA power multiplexing and multiCAP are employed in combination, reducing the assigned capacity to each user, but increasing the user density of the RAN and optimizing overall system throughput. In addition, the overall system throughput can be raised even more by employing power loading and narrower band guards [22] or employing single side-band transmissions [21].

The proposed NOMA-CAP technique [20] is experimentally validated on a W-band RoF downlink using six 1.25 GHz wide multiCAP bands and two NOMA levels with quadrature phase shift keying (QPSK) achieving an aggregated transmission rate of 30 Gbit/s. The two scenarios shown in Fig. 1 have been evaluated, where either two users use all the multiCAP bands and evenly share the capacity of the RAN or twelve users are multiplexed employing NOMA and multiCAP. The transition between scenarios—or any intermediate scenario—is dynamic depending on user demands and showcases the flexible resource provisioning that NOMA-CAP can provide to the RAN. This proof of concept shows two possible operation cases of NOMA-CAP, showing the trade-off between the number of users and the per-user capacity. These scenarios have been tested on a W-band RoF link as a demonstration of the high throughput employing the future 5G frequency ranges, although the NOMA-CAP technique is carrier independent and it could be operated in the traditional frequency ranges used for mobile communications.

The remainder of this paper is structured as follows: section II discusses NOMA and CAP as well as their combination to NOMA-CAP, while section III describes the experimental setup used for validation of NOMA-CAP in W-band; section IV shows experimentally obtained transmission results and their relation to 5G networks; finally, section V summarizes and concludes the paper.
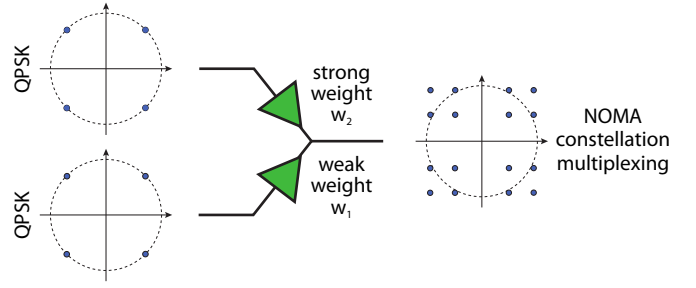
II. MULTI-BAND CARRIERLESS AMPLITUDE PHASE MODULATION WITH NON-ORTHOGONAL MULTIPLE ACCESS

This section provides a short discussion of the concepts of non-orthogonal multiple access (NOMA) and carrierless amplitude phase modulation (CAP) before discussing their combination into NOMA-CAP as proposed in this paper.

A. Non-Orthogonal Multiple Access

The NOMA power multiplexing technique multiplexes the data of several users in the power domain by combining the contributing signals and it is fully compatible with time- or frequency multiplexing. Successive interference cancellation (SIC) is employed in the terminal units in order to recover the contributing signals and thus demultiplex the different NOMA users data [13]. In wireless communications this technique may exploit the near-far effect, causing asymmetrical channel gains between the users [11].

NOMA power multiplexing is applied at the symbol level and a NOMA constellation for two users—as shown in Fig. 2—is obtained by assigning different weights to the user symbols before directly adding them:

$$x_{\text{NOMA}} = w_1 x_1 + w_2 x_2 \qquad (1)$$

where x_{NOMA} is the multiplexed signal for two NOMA users, w_1 and x_1 are the weight and symbol of the close user, while w_2 and x_2 are the weight and symbol of the far user. The weights are calculated in order to obtain the desired power ratio r_{Power} between users in the multiplexed signal.

$$r_{\text{Power}} = 20 \log \left(\frac{w_2}{w_1} \right) \qquad (2)$$

The user located closer to the base station (BS), i.e., receiving a higher multiplexed signal quality, will be assigned a weak weight in the multiplexed symbol and will implement SIC to remove the higher power signal for the far user, as depicted in Fig. 3. During SIC the user first decodes the undesired, stronger signal intended for the far user and subtracts it from the received signal, after which the desired weaker signal may be decoded. The user located far from the BS, i.e., with a lower received signal quality, will be assigned a stronger weight and thus the high power signal within the multiplexed symbol and will only decode their own signal [12], [15].

In the case of more than two users, SIC is implemented iteratively, decoding the largest power within the received
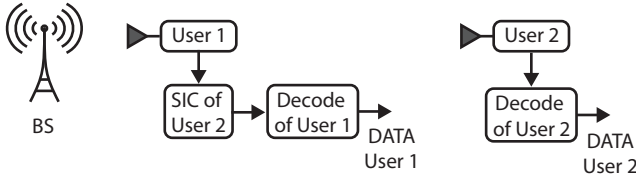
Fig. 3. NOMA receivers for two users with SIC employed by user 1 to remove the signal of user 2 before decoding its own signal.
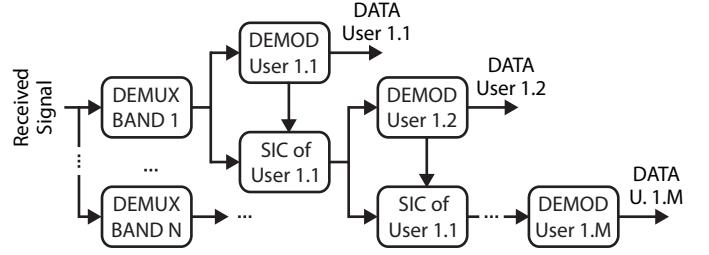

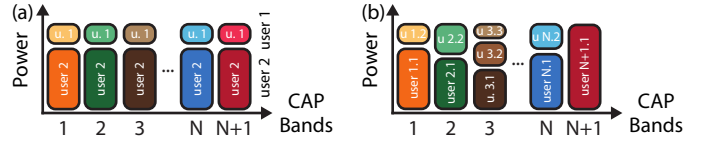Fig. 4. NOMA-CAP with multiCAP band separation and SIC receiver.

Fig. 5. Power multiplexing using NOMA and multiCAP: (a) NOMA multiplexing of two users employing all multiCAP bands, (b) multiple users are multiplexed employing NOMA and multiCAP.

multiplexed signal and subtracting it from the received signal until the signal of interest is the strongest in the remaining signal so it is possible to finally decode the data.

B. Multi-Band Carrierless Amplitude Phase Modulation

CAP is a scheme that, like quadrature amplitude modulation (QAM), transmits two streams of data separately by means of two orthogonal signals, namely the in-phase (I) and quadrature (Q) components. Additionally, a special feature of CAP modulation is the use of a pulse shaping function to significantly improve the spectral efficiency of the system. Unlike QAM, the generation of the CAP signal is not achieved by modulating two orthogonal carriers with the same frequency (i.e., sine and cosine). Instead two orthogonal filters are used to generate the two components of the signal. These filters are the result of the time-domain multiplication of the pulse shaping function and two orthogonal carriers. In this paper, the root raised cosine (RRC) pulse shaping function is employed to generate the filters, allowing the receiver to use a pair of matched filters with the same shape to retrieve the signal. Therefore, by combining the transmitter and the receiver, the complete response of the filters has the characteristics of a raised cosine (RC) function, which minimizes intersymbol interference (ISI).

CAP modulation, as many other modulation schemes, requires a flat frequency response of the transmission link to ensure good performance. In order to mitigate this impairment, the multi-band CAP (multiCAP) has been proposed for wireless and optical links, achieving high spectral efficiency over large bandwidths [23], [24]. By splitting the spectrum into sub-bands, multiCAP modulation enables the use of bit- and power-loading techniques for each band independently [18], according to its signal to noise ratio (SNR). Thus, with an adequate number of sub-bands, non-flat frequency responses (e.g. uneven antenna gain or non-flat frequency response of devices) can be alleviated to maximize spectral efficiency.

C. Non-Orthogonal Multiple Access with Multi-Band Carrierless Amplitude Phase Modulation

In this article, NOMA power multiplexing is combined with multiCAP modulation to enhance the capacity and flexibility of the RAN. System capacity is increased by reaping the benefits of multiCAP, optimizing the signal to channel conditions, while both multiCAP and NOMA lend themselves ideally to flexible and adaptive user provisioning.

At the transmitter NOMA power multiplexing is applied at the constellation level for each multiCAP band independently and before generation of the multiCAP signal. NOMA-CAP

reception will require the extraction of each multiCAP band—employing its matched filters—and then the SIC process to extract the signal of interest. If several NOMA users have been multiplexed, the SIC process will be applied iteratively after multiCAP demultiplexing until the user signal of interest is demodulated, as is shown in Fig. 4.

The combination of NOMA and multiCAP allows a dynamic assignment of the resources to fulfill the user demands. For example, in a low density user distribution scenario, such as shown in Fig. 5(a), the users can use all multiCAP bands simultaneously while their data is multiplexed by NOMA. In this scenario, the users equally share the maximum available capacity of the RAN. If the number of users increases, NOMA multiplexing can be applied independently to each multiCAP band (with potentially different numbers of users per band) and bands can be assigned to different groups of users, as shown in Fig. 5(b). This enables a flexible distribution of the RAN capacity over many users and avoids blocking new users to a large degree.

In the next section, a NOMA-CAP system employing two levels of NOMA with QPSK signals and six 1.25 GHz multiCAP bands is proposed and demonstrated. The proposed NOMA-CAP system may provide an aggregated transmission rate of 30 Gbit/s and has been evaluated in two different scenarios. In the fist scenario—a low user density scenario—the capacity of the RAN is distributed between two users employing NOMA-CAP, as in Fig. 5(a), to obtain 15 Gbit/s per user. In the second scenario, twelve users are multiplexed using NOMA-CAP, similar to Fig. 5(b), where the different multiCAP bands carry different users, and the RAN capacity is divided evenly among all users to obtain 2.5 Gbit/s per user.

III. SETUP

The experimental setup used to evaluate the proposed NOMA-CAP transmission over a hybrid photonic-wireless downlink follows the concepts of a C-RAN with analog RoF fronthaul [3], [4] and mm-wave radio access units (RAUs) of reduced complexity [8]. The setup—schematically shown in
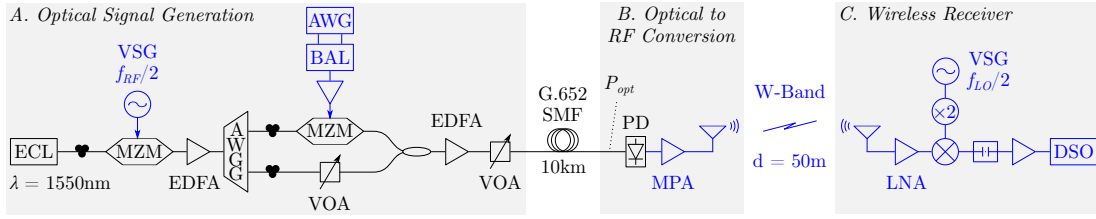
Fig. 6. Schematic of the experimental setup; ECL: external cavity laser, MZM: Mach-Zehnder modulator, VSG: vector signal generator, RF: radio frequency, EDFA: erbium doped fiber amplifier, AWGG: arrayed waveguide grating, AWG: arbitrary waveform generator, BAL: balun, VOA: variable optical attenuator, SMF: standard single mode fiber, PD: photodiode, MPA: medium power amplifier, LNA: low noise amplifier, LO: local oscillator, DSO: digital storage oscilloscope.

Fig. 6 and previously tested on [21], [22], [25]—consists of three stations, linked by optical fiber and wireless transmission respectively: Optical Signal Generation, Optical to RF Conversion and Wireless Receiver. The *A. Optical Signal Generation* is the equivalent of the central office (CO) and generates an optical signal with two spectral lines spaced at the frequency of the radio carrier $f_{RF} = 84\,\text{GHz}$. The signal carries the NOMA-CAP signal and links via an analog RoF system over 10 km of standard single mode fiber (SMF) to *B. Optical to Radio Frequency Conversion* in the RAU, from where the signal is wirelessly delivered to *C. the Wireless Receiver*. The latter recovers the RF signal, translates it to baseband and performs the DSP required to decode the NOMA-CAP signal. The different stations are described in detail in the following sections.

A. Optical Signal Generation

The optical output of a narrow linewidth external cavity laser (ECL) at $\lambda = 1550\,\text{nm}$ is modulated by a Mach-Zehnder modulator (MZM) biased at its minimum transmission point with a sinusoidal signal at $f_{\text{RF}}/2$ obtained from a vector signal generator (VSG). This configuration generates the basic optical signal for photonic generation of the RF signal with two spectral lines spaced at f_{RF}. After amplification in an erbium doped fiber amplifier (EDFA), the lines are separated in an arrayed waveguide grating (AWGG) demultiplexer before modulating of one of them with the NOMA-CAP signal.

The block diagram for the digital signal processing (DSP) to generate the NOMA-CAP signal is shown in Fig. 7. First, the user data—pseudo random bit sequences (PRBSs) of length $2^{11} - 1$—are distributed among all the assigned multiCAP bands (varying between one and all available bands) and are QPSK mapped for each NOMA level. The two NOMA levels are power weighted and added for each multiCAP band before the band signals are upsampled and filtered using a pair of band specific multiCAP orthogonal filters. In all scenarios a total of six multiCAP bands of 1.25 GHz width are used. Finally, these signals are aggregated into the full transmitted NOMA-CAP signal.

The latter is generated with an arbitrary waveform generator (AWG), converted to single-ended with a balun (BAL) and amplified to achieve a voltage swing able to modulate one of the spectral lines in a second MZM. The power of the other spectral line is adjusted with a variable optical attenuator (VOA) to ensure equal power of both spectral lines. A second EDFA amplifies the signal for transmission, while a second
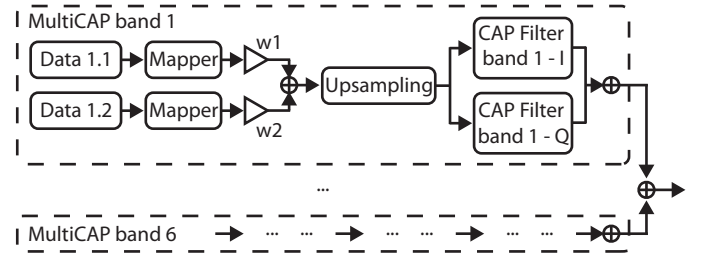

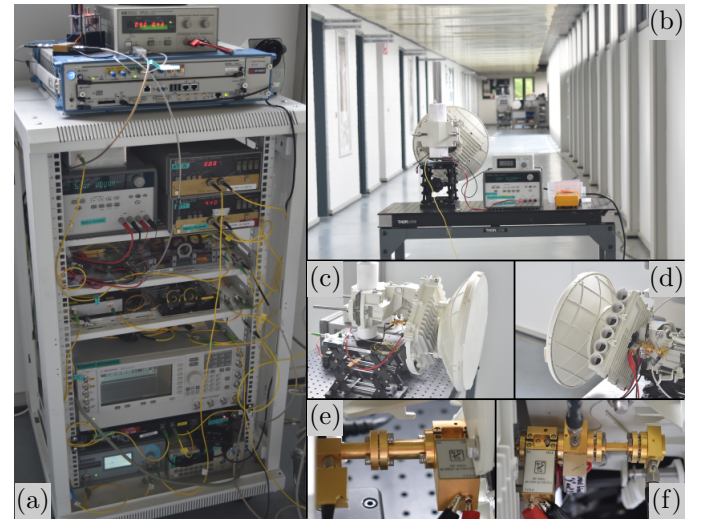Fig. 7. Transmitter DSP block diagram for NOMA-CAP signal generation.

Fig. 8. Laboratory setup for NOMA-CAP transmission in W-band; (a) optical signal generation, (b) optical to RF conversion station and transmission path, (c)–(d) transmitter and receiver parabolic antennas, (e) PD and MPA at optical to RF conversion, (f) LNA, mixer and frequency doubler at the wireless receiver.

VOA controls the launched power and thus the power at the optical to RF conversion stage after transmission through 10 km of ITU-T G.652 SMF.

For laboratory convenience the optical signal generation is housed in a half-size rack, shown in Fig. 8(a).

B. Optical to Radio Frequency Conversion

Optical to RF conversion is performed by a RAU designed for minimum complexity, consisting only of a high-speed photodiode (PD), a single medium power amplifier (MPA) and the transmitter antenna. The RF signal is generated through the beating of the two optical lines on a PD that features a 3 dB bandwidth of 90 GHz and a responsivity of 0.5 A/W.
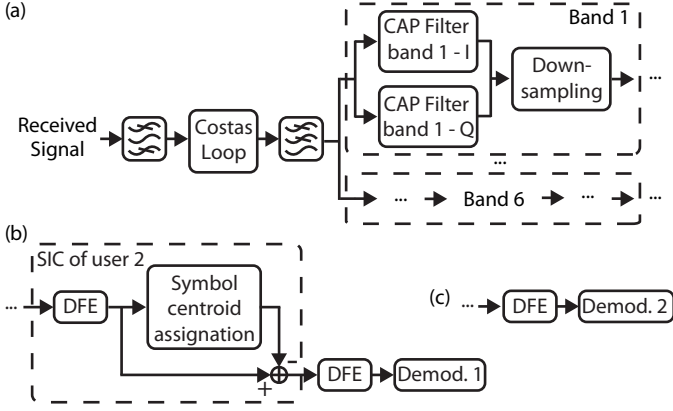
Fig. 9. Receiver DSP block diagram: (a) multiCAP band recovery (common to all receivers), (b) user type 1 receiver with SIC processing, (c) user type 2 receiver without SIC processing.
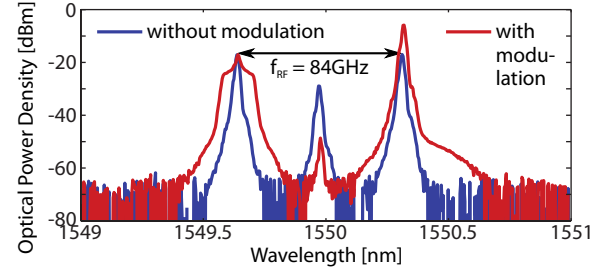

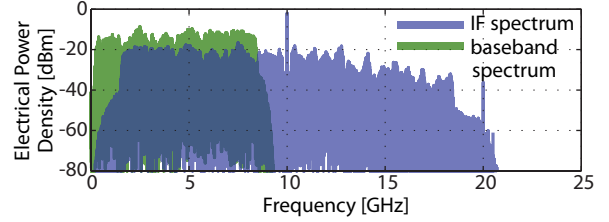Fig. 10. Optical spectra of the two spectral lines generated with the first MZM before and after modulation.

Fig. 11. Electrical spectra of the received IF signal (top) and the received baseband signal after Costas loop (bottom).

The variable incoming optical power allows for generation of different RF powers which are amplified by 10 dB by the MPA up to a saturation output power of 12 dBm; PD and MPA, are shown in Fig. 8(e). A parabolic antenna with a gain of 48 dBi is used to transmit the signal to the wireless receiver as shown in Figs. 8(b) and (c) respectively.

C. Wireless Receiver and Signal Processing

At the receiver an identical antenna—shown in Fig. 8(d)—recovers the RF signal which is amplified by 20 dB using a low noise amplifier (LNA) before its downconversion in a balanced mixer to an intermediate frequency (IF) at $f_{IF} = f_{RF} - f_{LO} = 10$ GHz. The local oscillator (LO) for the mixer is obtained from a passive frequency doubler, driven with a sinusoid at $f_{LO}/2$ from a second VSG; the combination of LNA, mixer and frequency doubler is shown in Fig. 8(f). The resulting IF signal is DC blocked and amplified before it is recorded on a digital storage oscilloscope (DSO) for offline processing.

The receiver signal processing block diagram is shown in Fig. 9 and consists of a band-pass filter for noise bandwidth reduction and a Costas loop [26] for carrier frequency and phase recovery for IF to baseband conversion. The baseband signal is low-pass filtered and each multiCAP band is extracted, employing the pair of orthogonal filters for the band of interest, as described in section II-B; this part is common to all the receivers and is shown in Fig. 9(a). The close users further implement SIC as is shown in Fig. 9(b), in order to remove the far users' data. The first step of the SIC consists of a decision feedback equalizer (DFE) with 30 forward and 20 backward taps, after which the symbol centroid of the interfering user's signal is calculated employing the k-means algorithm [18]. Finally, the symbol centroid of the far user is subtracted from the equalized signal. After SIC, the DFE is applied again to the new signal and finally the signal is demapped. In the case of farther users, SIC is not required and the DFE and demapping are performed directly, as shown in Fig. 9(c).

IV. EXPERIMENTAL RESULTS

This section discusses the results of applying NOMA-CAP in a W-band RoF link, proving the functionality and applicability

of NOMA-CAP for 5G networks. First, optical and electrical spectra at different stages of the experimental system are shown and discussed. Then the system transmission performance is evaluated through bit error rate measurements in two scenarios with different numbers of users and for varying NOMA-CAP parameters. Finally, the results and their applicability are discussed.

A. Signal Generation and Reception

Fig. 10 depicts the optical spectrum after the first MZM, clearly showing the two spectral lines separated by $f_{RF} = 84$ GHz. The optical spectrum after modulating one of these two spectral lines previous to their transmission along the fiber is also shown. In Fig. 11, the electrical spectrum of the received signal after the analog downconversion to IF and digital downconversion to baseband is shown. The electrical spectra allow recognition of the multiCAP bands, but show severe and non-uniform impairments from the wireless channel, receiver electrical response and the downconversion process itself. This effect can be partly corrected by a passband filter before the Costas loop, removing the upper side band of the signal that is the most distorted.

B. System Transmission Performance

For the analysis of transmission performance, the received optical power on the PD is varied between -3 dBm and 2.5 dBm using the second VOA while the wireless distance remains constant (50 m). This optical power is directly related with the transmitted RF power, so its variation can be used to emulate the wireless distance without moving the antennas [27]. The power ratio between users is defined as in Eq. (2) and the total power of the digitally generated NOMA-CAP signal is kept constant. The analysis of distance has been performed employing the respective BER limits of 3.8×10^{-3}
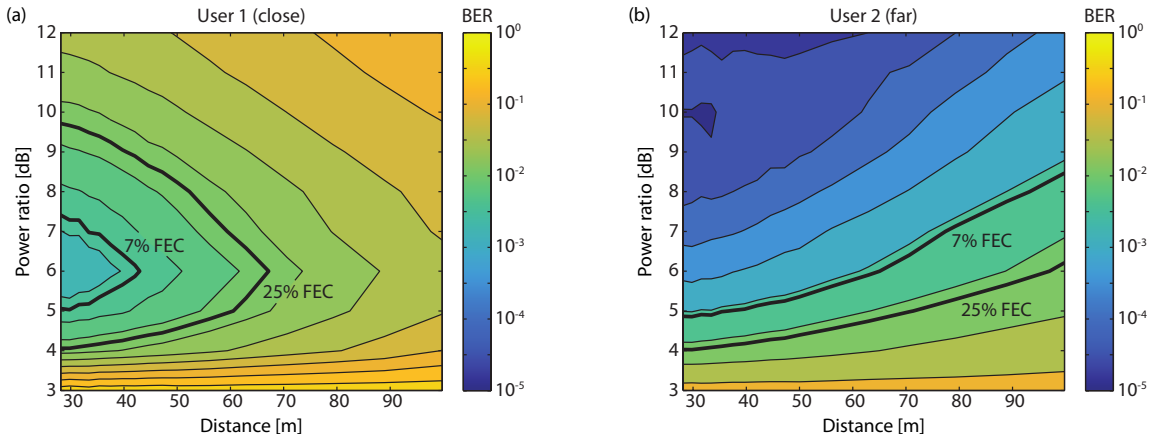
Fig. 12. BER maps in terms of distance and power ratio for (a) the close by user and (b) the user located far from the transmitting antenna.

TABLE I
SUMMARY OF MAXIMUM ACHIEVABLE DISTANCES FOR BOTH USERS
AND DIFFERENT POWER RATIOS.

Power-ratio	User 1 (close)		User 2 (far)	
	Distance* (7% FEC)	Distance (25% FEC)	Distance† (7% FEC)	Distance† (25% FEC)
5dB	×	61m	36m	70m
6dB	43m	67m	65m	96m
7dB	33m	59m	77m	○
8dB	×	52m	○	○
9dB	×	40m	○	○

* × denotes cases where no transmission below BER limit for the respective FEC could be achieved.

† ○ denotes cases where distance greater than those experimentally tested is expected to be achievable.

Fig. 13. Achievable distances and required FEC overhead for the two users at different power ratios

and 1.32×10^{-2} for standard forward error corrections (FEC) with 7 % and 25 % overhead (OH) [28].

System transmission BER performance in the first scenario with only two users present—similar to the low density user distribution scenario in Fig.1(a)—is shown in Fig. 12, where BER is plotted in terms of wireless distance and power ratio r_{Power} between the close and the far user. Both users employ all six bands available and share the full system capacity—i.e., 15 Gbit/s each. For user 2—i.e., the user located far from the transmitting antenna—the NOMA multiplexing with the signal of user 1 will be regarded as an increment of the received noise and thus a reduction of the power ratio between users will increase the user BER and reduce the achievable distance for user 2 as is seen in Fig. 12(b). The user 2 would thus prefer a scenario with high power ratio since with power ratios above 8 dB a BER below the limit for a 7% OH FEC is achieved for all analyzed distances.

In the same scenario, user 1—i.e., the user close to the transmitting antenna—will apply SIC cancellation before demodulation in order to remove the signal of user 2. Any errors in the calculation of the centroid of user 2 will affect the decoding of user 1 in the SIC process and thus they will cause a higher BER. An increase in the transmission distance for user 1 will result in an increase in the number of errors in the centroid calculation, causing an increase in BER of user 1, as
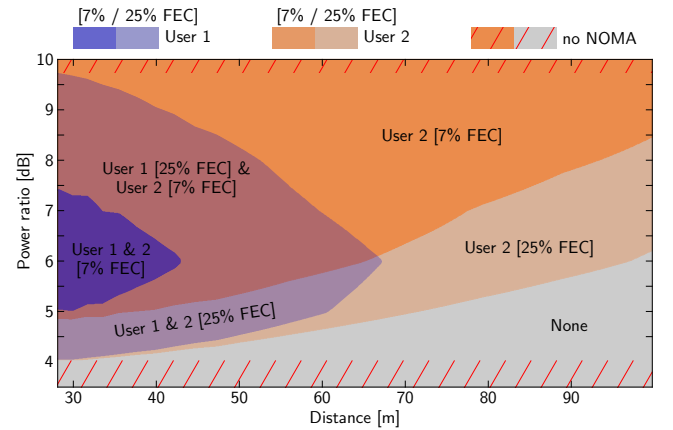
can be seen in Fig. 12(a). The use of a low power ratio between users—i.e., the power of user 1 and user 2 are comparable—will have a similar effect as placing user 1 at a long distance, resulting in errors in the calculation of the user 2 centroid and consequently transmitting the error to user 1 decoding. On the other hand, the BER of user 1 will also increase with high power ratios as the signal will be too weak after SIC, even if the SIC process perfectly calculates the user 2 centroids. In consequence, user 1 will only be successfully demodulated for intermediate power relations and for close distances, as seen in Fig. 12(a).

Table I summarizes the maximum reachable distances for both users under different power ratios. When the power ratio is 6 dB and a 7% OH FEC is assumed, user 1 can be placed as far as 43 m and the user 2 at up to 65 m. If the user 2 needs to be placed further, the power ratio can be changed to 7 dB and the user 2 could be placed as far as 77 m, but the distance of user 1 will have to be reduced and cannot be greater than 33 m. Therefore, the increment of the operational range of one user will decrease the range of the other user. If the effective data rate can be reduced, a 25% OH FEC can be implemented and both users can be placed farther. In this case, user 1 can be placed at 67 m and user 2 at 96 m with a power ratio of 6 dB
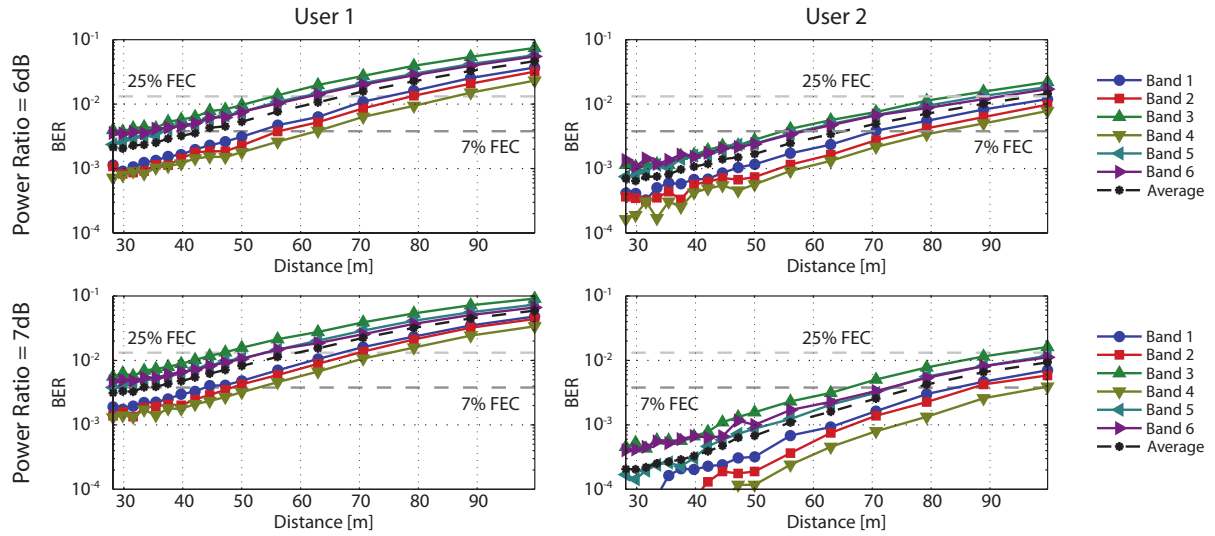
Fig. 14. BER over wireless distance for different multiCAP bands, each carrying a close and a far user multiplexed with NOMA.

TABLE II
SUMMARY OF MAXIMUM ACHIEVABLE DISTANCES FOR EACH MULTICAP
BAND AND BOTH USER TYPES WITH POWER RATIOS OF 6 DB AND 7 DB.

Power-ratio [dB]	User Type	FEC OH [%]	MultiCAP Band*†					
			#1 [m]	#2 [m]	#3 [m]	#4 [m]	#5 [m]	#6 [m]
6	close	7	53	47	30	63	36	34
		25	75	79	55	86	61	61
	far	7	70	78	56	82	59	59
		25	○	○	84	○	89	91
7	close	7	44	49	×	53	30	×
		25	67	70	47	75	54	54
	far	7	84	87	66	99	73	73
		25	○	○	93	○	○	○

* × denotes cases where no transmission below BER limit for the respective
FEC could be achieved.
† ○ denotes cases where distance greater than those experimentally tested
is expected to be achievable.

while for 7 dB the far user achieves distances beyond those measured. The power ratio between the user signals will thus allow adapting the system to the required range as is seen in Fig. 13 which illustrates the achievable distances (and required FEC overhead) for the two users for different power ratios.

The BER of each multiCAP band and the average BER are shown in Fig. 14 in terms of distance of near and far users with power ratios of 6 dB and 7 dB. Fig. 14 is used to study a second scenario with twelve users, six users of type 1 and six users of type 2, with a capacity of 2.5 Gbit/s per user. These users are multiplexed employing NOMA and all the multiCAP bands, similar to the scenario described in Fig. 1(b).

The BER of each multiCAP band in terms of user distance and power ratio shows a similar behavior to that previously described for a NOMA-CAP system where all bands are employed by the same users. The maximum distances for both types of users and for each multiCAP band are summarized in Table II for both FEC types and for power ratios of 6 dB and 7 dB. The BER of each band is different due to the differing channel

and system impairments and thus in this scenario some of the bands (1, 2 and 4) allow longer distances while other bands (3, 5 and 6) are limited to shorter distances.

If the user capacity is kept stable—i.e., only the 7% OH FEC is used—band 3 and 6 will not allow the use of a power ratio of 7 dB since users of type 1 in these bands cannot obtain a BER below the respective FEC limit. The remaining bands may be used with both power ratios, depending on the necessities and position of the different users. Therefore, an optimal accommodation of the users in different multiCAP bands is possible by adjusting the NOMA power ratio in each band independently.

Finally, Fig. 15 shows the constellation diagrams for all multiCAP bands and for both types of NOMA users, given a power relation of 6 dB and a distance of 30 m. The constellation multiplexing can be observed with the symbols of user 1 visibly superimposed on the symbols of user 2. For user 1 the symbols of user 2 have been removed with the SIC process and only the desired symbols are observed.

V. CONCLUSIONS

A combination of multiCAP modulation and NOMA multiplexing was suggested for application in future 5th generation mobile RANs, allowing the optimization of the available capacity as well as flexible user provisioning. An experimental demonstration was given for a NOMA-CAP RoF system in the W-band, analyzing BER in two different scenarios with different user density.

The experimental demonstration achieved an aggregate system capacity of 30 Gbit/s using a NOMA-CAP signal consisting of six bands with a width of 1.25 GHz each. BER measurements are shown for different power ratios between the contributing NOMA signals and for different optical power, relating to wireless distances between 30 m and 100 m. Power ratios close to 6 dB are found to be optimum and in a two user scenario allow distances of 43 m and 65 m respectively, with BER values below the limit for a standard FEC with 7% OH.
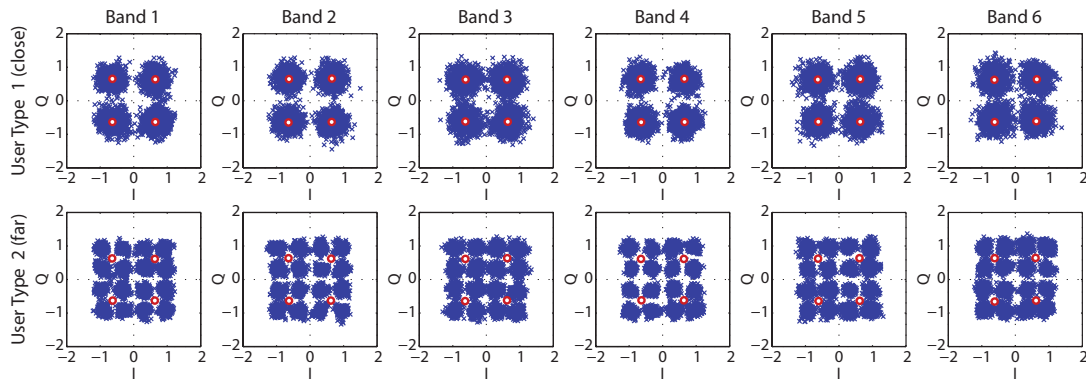
Fig. 15. Received constellations for both types of NOMA users and the six multiCAP bands for a power ratio of 6 dB and a distance of 30 m.

The introduction of NOMA-CAP over W-band RoF allows the RAN to dynamically adapt itself to varying user data rate demands and user densities. This flexible multi-user provisioning will also permit to change the data rate provided to the current users to grant access to new users in the RAN. In a low user density scenario, a high data rate can be provided to the users. If new users need to be served by the RAN, the delivered data rate can be reduced, independently assigning the multiCAP bands to these new users and avoiding blocking to a maximum degree. The experimental demonstration of these situations proves the operation with two users with 15 Gbit/s data rate each or twelve users with 2.5 Gbit/s each, showing the trade-off between the number of users and per-user capacity. The number of users could be raised with an increment of the number of multiCAP bands and NOMA levels, but causing a reduction of the per-user capacity.

REFERENCES

[1] M. Fiorani et al., "Challenges for 5G transport networks," in Proc. ANTS 2014, 2014.
[2] T. Pfeiffer, "Next generation mobile fronthaul and midhaul architectures," IEEE J. Opt. Commun. Netw., vol. 7, no. 11, pp. B38–B45, 2015.
[3] P. Rost et al., "Cloud technologies for flexible 5G radio access networks," IEEE Commun. Mag., vol. 52, no. 5, pp. 68–76, 2014.
[4] C. Liu et al., "A novel multi-service small-cell cloud radio access network for mobile backhaul and computing based on radio-over-fiber technologies," J. Lightw. Technol., vol. 31, no. 17, pp. 2869–2875, 2013.
[5] K. Kitayama, T. Kuri, J. Vegas Olmos, and H. Toda, "Fiber-wireless networks and radio-over-fibre technique," in Proc. CLEO 2008, 2008, paper CThR4.
[6] S. Rommel et al., "W-band photonic-wireless link with a Schottky diode envelope detector and bend insensitive fiber," Opt. Express, vol. 24, no. 11, pp. 11 312–11 322, 2016.
[7] J. Wells, "Faster than fiber: The future of multi-G/s wireless," IEEE Microw. Mag., vol. 10, no. 3, pp. 104–112, 2009.
[8] S. Rodríguez, S. Rommel, J. J. Vegas Olmos, and I. Tafur Monroy, "Reconfigurable radio access unit to dynamically distribute W-band signals in 5G wireless access networks," Opt. Switch. Netw., vol. 24, pp. 21–24, 2017.
[9] F. Lu et al., "Non-orthogonal multiple access with successive interference cancellation in millimeter-wave radio-over-fiber systems," J. Lightw. Technol., vol. 34, no. 17, pp. 4179–4186, 2016.
[10] Ł. Chorchos et al., "Reconfigurable radio access unit for DWDM to W-band wireless conversion," IEEE Photonics Technol. Lett., vol. 29, no. 6, pp. 489–492, 2017.
[11] L. Dai et al., "Non-orthogonal multiple access for 5G: solutions, challenges, opportunities, and future research trends," IEEE Commun. Mag., vol. 53, no. 9, pp. 74–81, 2015.
[12] A. Benjebbour et al., "Concept and practical considerations of non-orthogonal multiple access (NOMA) for future radio access," in Proc. ISPACS 2013, 2013, pp. 770–774.
[13] K. Higuchi and A. Benjebbour, "Non-orthogonal multiple access (NOMA) with successive interference cancellation for future radio access," IEICE Trans. Commun., vol. E98-B, no. 3, pp. 403–414, 2015.
[14] Z. Ding, Z. Zhao, M. Peng, and H. V. Poor, "On the spectral efficiency and security enhancements of NOMA assisted multicast-unicast streaming," IEEE Trans. Commun., vol. 65, no. 7, pp. 3151–3163, 2017.
[15] T. Manglayev, R. C. Kizilirmak, and Y. H. Kho, "Optimum power allocation for non-orthogonal multiple access (NOMA)," in Proc. AICT 2016, 2016.
[16] Z. Chen, Z. Ding, X. Dai, and R. Zhang, "An optimization perspective of the superiority of NOMA compared to conventional OMA," IEEE Trans. Sig. Process., vol. 65, no. 19, pp. 5191–5202, 2017.
[17] V. Sipal et al., "Adaptive OFDM for wireless interconnect in confined enclosures," IEEE Wireless Commun. Lett., vol. 2, no. 5, pp. 507–510, 2013.
[18] M. I. Olmedo et al., "Multiband carrierless amplitude phase modulation for high capacity optical data links," J. Lightw. Technol., vol. 32, no. 4, pp. 798–804, 2014.
[19] J. L. Wei et al., "Performance and power dissipation comparisons between 28 Gb/s NRZ, PAM, CAP and optical OFDM systems for data communication applications," J. Lightw. Technol., vol. 30, no. 20, pp. 3273–3280, 2012.
[20] J. A. Altabas et al., "Non-orthogonal multiple access and carrierless amplitude phase modulation for 5G mobile networks," in Proc. ECOC 2017, 2017, paper Tu.1.B.2.
[21] R. Puerta, S. Rommel, J. J. Vegas Olmos, and I. Tafur Monroy, "Optically generated single side-band radio-over-fiber transmission of 60Gbit/s over 50m at W-band," in Proc. OFC 2017, 2017, paper M3E.4.
[22] S. Rommel, R. Puerta, J. J. Vegas Olmos, and I. Tafur Monroy, "Capacity enhancement for hybrid fiber-wireless channels with 46.8Gbit/s wireless multi-CAP transmission over 50m at W-band," in Proc. OFC 2017, 2017, paper M3E.5.
[23] R. Puerta, S. Rommel, J. J. Vegas Olmos, and I. Tafur Monroy, "Up to 35Gbps ultra-wideband wireless data transmission links," in Proc. PIMRC 2016, 2016.
[24] R. Puerta et al., "Effective 100Gb/s IM/DD 850nm multi- and single-mode VCSEL transmission through OM4 MMF," J. Lightw. Technol., 2016.
[25] L. C. P. Cavalcante et al., "Performance evaluation of wavelet-coded OFDM on a 4.9 Gb/s W-band radio-over-fiber link," J. Lightwave Technol., vol. 35, no. 14, pp. 2803–2809, 2017.
[26] J. P. Costas, "Synchronous communications," Proc. IRE, vol. 44, no. 12, pp. 1713–1718, 1956.
[27] S. Rommel et al., "Outdoor W-band hybrid photonic wireless link based on an optical SFP+ module," IEEE Photonics Technol. Lett., vol. 28, no. 21, pp. 2303–2306, 2016.
[28] ITU-T G.975.1, "Forward error correction for high bit-rate DWDM submarine systems," 2004.